Published on 04 December 2018. Downloaded by California Institute of Technology on 1/31/2019 7:33:55 PM.

Soft Matter

COMMUNICATION

View Article Online
View Journal | View Issue

Check for updates

Cite this: *Soft Matter*, 2018, **14**, 9744

Received 11th October 2018,
Accepted 19th November 2018

DOI: 10.1039/c8sm02082e

rsc.li/soft-matter-journal

Shape-morphing architected sheets with non-periodic cut patterns†

Paolo Celli, *[a] Connor McMahan,[a] Brian Ramirez,[a] Anton Bauhofer,[ab] Christina Naify,[c] Douglas Hofmann,[c] Basile Audoly [ad] and Chiara Daraio *[a]

We investigate the out-of-plane shape morphing capability of single-material elastic sheets with architected cut patterns that result in arrays of tiles connected by flexible hinges. We demonstrate that a non-periodic cut pattern can cause a sheet to buckle into three-dimensional shapes, such as domes or patterns of wrinkles, when pulled at specific boundary points. These global buckling modes are observed in experiments and rationalized by an in-plane kinematic analysis that highlights the role of the geometric frustration arising from non-periodicity. The study focuses on elastic sheets, and is later extended to elastic-plastic materials to achieve shape retention. Our work illustrates a scalable route towards the fabrication of three-dimensional objects with nonzero Gaussian curvature from initially-flat sheets.

Imparting elastic sheets with a mesoscale architecture enables the creation of materials with unusual characteristics, such as extreme extensibility,[1] deployability[2,3] and auxeticity.[4,5] These properties can be leveraged to design sheets that morph into complex three-dimensional objects. For example, origami sheets can be turned into nearly-arbitrary shapes,[6–9] but are typically challenging to fold[10] or actuate.[11–13] Patterned elastomeric sheets,[14–19] bilayers[20] and sheets with smart hinges[21–23] can morph into three-dimensional surfaces with nonzero Gaussian curvature *via* non-mechanical stimuli, but their fabrication is complex. Ribbon- and membrane-like flat mesostructures can buckle out of plane and produce three-dimensional geometries when subject to mechanical actuation.[24–27] However, compressive actuation requires non-trivial assembly processes, and the geometries obtained with tensile loads are limited to thin, arch-like features.

In contrast to shape-morphing origami or bilayer films, sheets with architected cut patterns can be easily fabricated *via* subtractive technologies. Their out-of-plane deformation can be triggered by manual forming,[28–30] by actuating smart hinges,[31] or by applying compressive boundary loads.[25,32,33] Recently, it has been demonstrated that sheets with periodic perforations can also buckle locally in tension,[27,34–37] producing crease patterns that can be used for soft robotic locomotion[38] or as coatings for sunlight control.[37] However, since these buckling modes take place at the scale of the unit cells, the size of the transverse features they can produce cannot significantly exceed the typical length of the cuts. Non-periodic cut patterns have been seldom explored in this context: non-periodicity is known to lead to geometric frustration,[39,40] *i.e.*, the desired deformation mode is impeded by the geometric incompatibility between neighboring cells. In the few cases where non-periodic cut patterns have been explored, frustration has been avoided.[41–44] In particular, the effect of geometric frustration on the out-of-plane deformations of thin architected sheets has been ignored so far.

In this work, we study the tensile response of elastic sheets featuring non-periodic cut patterns, and intentionally leverage geometric frustration to induce controllable, global shape changes *via* buckling. In most of our designs, we use point-like boundary loads that induce large deformations in selected sub-domains of the sheets. The inhomogeneous distribution of strains results in global buckling modes that make the sheets bend out of plane and morph into dome-like surfaces with nonzero Gaussian curvature and patterns of wrinkles confined to pre-determined regions. Note that a similar mechanism is at work in the morphogenesis of living systems due to differential growth.[45–47] We also extend the method to initially-cylindrical sheets and to cut patterns arranged into non-rectangular grids, and demonstrate the formation of persistent three-dimensional surfaces *via* elastic-plastic materials.[36] Our work distinguishes itself for the simplicity of fabrication and actuation, and for its potential applicability to material and structural systems at

[a] *Department of Mechanical and Civil Engineering, California Institute of Technology, Pasadena, CA 91125, USA. E-mail: pcelli@caltech.edu, daraio@caltech.edu*
[b] *Department of Mechanical and Process Engineering, ETH Zurich, 8092 Zurich, Switzerland*
[c] *Jet Propulsion Laboratory/California Institute of Technology, Pasadena, CA, 91109, USA*
[d] *Laboratoire de Mécanique des Solides, CNRS, UMR 7649, Département de Mécanique, École Polytechnique, 91128 Palaiseau CEDEX, France*

† Electronic supplementary information (ESI) available. See DOI: 10.1039/c8sm02082e

This journal is © The Royal Society of Chemistry 2018

Published on 04 December 2018. Downloaded by California Institute of Technology on 1/31/2019 7:33:55 PM.

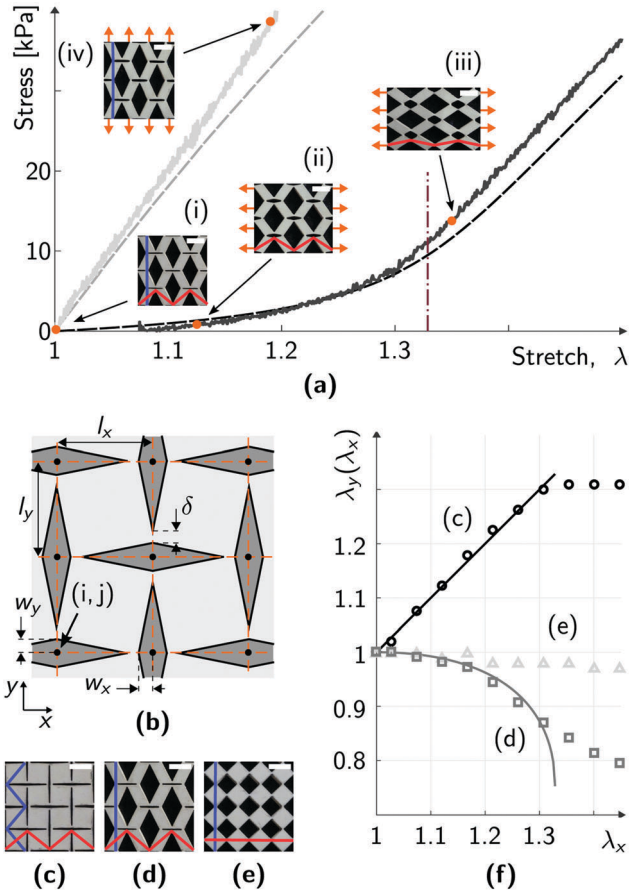

Fig. 1 In-plane response of periodic sheets. (a) Uniaxial response of the sheet with undeformed geometry shown in (i): horizontal loading (black lines) and vertical loading (grey lines), experiments (solid lines) and FE simulations (dashed lines). The vertical dash-dot line is the geometric-to-elastic transition predicted by kinematics. Insets (i–iv) show snapshots of a 4 × 4-tile portion of the sheet at different levels of deformation. The red and blue overlaid lines are obtained by joining the diagonals in a particular row and column of tiles. (b) Sketch of a generic periodic architecture parameterized by design variables. (c–e) Details of three periodic undeformed specimens, corresponding to different values of (w_x, w_y) listed in the ESI.† (f) Transverse stretch λ_y as a function of the stretch along the loading direction, λ_x, for the same set of specimens: experiments (markers) and kinematic predictions (solid curves). Scale bar: 6 mm.

vastly-different scales; it therefore illustrates a potential path towards the high-throughput realization of morphable surfaces.

We start by analyzing a simple cut pattern featuring a large-amplitude, planar mode of deformation. A 108-by-108 mm, 1.55 mm-thick natural rubber sheet is laser-cut[48] following a pattern of diamond-shaped cut-outs and straight cut lines ending close to the diamonds' vertices. These two types of cuts are visible in black in the insets of Fig. 1. The result is an array of 18 × 18 rhomboid tiles connected by thin hinges. The experimental traction curves (Fig. 1(a)) for unaxial tension reveal a strongly anisotropic and non-linear behavior (see ESI† for details). When the tension is applied in the x-direction (horizontal direction in the figure, black lines) the response is initially compliant up to a stretch value $\lambda \sim 1.3$, and then becomes stiffer. When the tension is applied in the y-direction (vertical direction in the figure, gray lines), the response is stiff and approximately linear, without any compliant regime. We simulated the mechanical response of the architected sheet numerically, by using a finite element (FE) model for a neo-Hookean material in plane strain (an assumption justified in the ESI†). The numerical traction curves are in good agreement with the experimental ones (Fig. 1(a)).

The salient features of the loading curves can be explained by a kinematic analysis, in which the sheet is modeled as an array of rigid tiles connected by pin joints. Such networks can feature modes of deformation known as mechanisms,[49] which are mapped to low-energy configurations of the elastic sheet involving mainly bending and shear at the hinges.[50] A mechanism relies on the coordinated rotation of the tiles in response to applied tension (Fig. 1(a), ESI† and ref. 51 and 52). The maximum stretch attainable *via* a mechanism can be derived by considering the broken lines connecting the diagonals of the tiles in a given row or column—red and blue lines in Fig. 1(i). As the length of these lines is preserved by mechanisms, the maximum stretch in the x or y direction is attained when the corresponding line is fully stretched out. For the cut design used in Fig. 1(a), this maximum stretch is calculated by a geometric argument as $\lambda_x = 1.33$ in the x-direction, as indicated by the dash-dotted line in the figure; this is indeed where the compliant-to-stiff transition is observed in the traction curves. Conversely, the (blue) line of diagonals in the y-direction is straight by design, and no mechanism can be activated when the tension is applied in this direction; this is consistent with the absence of an initial compliant regime in the grey curves in Fig. 1(a).

Next, we introduce a family of periodic cut patterns parameterized by design variables. Our generic pattern, sketched in Fig. 1(b), is obtained by cutting out diamonds with alternating directions, centered at the nodes of a grid of $N_x \times N_y$ rectangles, each with dimensions $l_x \times l_y$. The two families of diamonds are assigned different widths, w_x and w_y, so that the previous design comprising line-cuts can be recovered as the special case $w_y = 0$. The length of the diamonds is such that a gap (hinge) of width δ is present between adjacent diamonds. Three examples of periodic geometries cut out in natural rubber sheets are shown in Fig. 1(c–e), for $N_x = N_y = 18$ and $l_x = l_y = 6$ mm; note that the shape of the tiles (light grey) can now vary from rhomboid to square. Experimental traction curves for three particular cutting patterns are plotted in the plane of stretches (λ_x, λ_y) in Fig. 1(f), and compared with the predictions of the kinematic analysis (see ESI†),

$$\lambda_y(\lambda_x) = \frac{d_v}{l_y}\sin\left[\gamma + \arccos\left(\frac{\lambda_x l_x}{d_h}\right)\right], \qquad (1)$$

where d_h and d_v are the lengths of the diagonals of a tile, and γ is the angle between these diagonals. The design variables have a strong influence on tension tests. The cut pattern in Fig. 1(c) gives rise to an auxetic mechanism[4] having a negative Poisson's ratio $\nu = -1$; this is reflected by the positive slope of the black curve in Fig. 1(e). By contrast, the mechanism associated with the cut pattern in Fig. 1(a and d) has a positive Poisson's ratio. For both these cut patterns, the kinematic

Published on 04 December 2018. Downloaded by California Institute of Technology on 1/31/2019 7:33:55 PM.

model provides an accurate prediction of the transverse stretch up to around $\lambda_x \sim 1.3$, where the joints start to stretch. Finally, the cut pattern in Fig. 1(e) is stiff when loaded in tension since the diagonals of adjacent tiles are aligned. The effect of the design parameters δ and t on the in-plane response is discussed in the ESI.†

Having analyzed a family of periodic cut patterns, we now investigate non-uniform designs, obtained by specifying values of w_x and w_y in every cell of a rectangular grid; the cell size $l_x \times l_y$ is uniform throughout the sheet. Upon deformation, we expect that every unit cell of these non-periodic sheets will try to follow the mechanism corresponding to the local values of w_x and w_y, as described by eqn (1). However, mechanisms corresponding to neighboring cells are not geometrically compatible in general (see ESI†). Thus, we investigate how this incompatibility is resolved at the global level by buckling. As a first example, we consider a cut geometry where w_x is constant while w_y varies sinusoidally in the y-direction, see Fig. 2(a), using a 1.55 mm-thick natural rubber sheet with $N_x = 36$, $N_y = 18$, $l_x = 6$ mm, $l_y = 2l_x$. This choice of maps for w_x and w_y ensures that the top and bottom parts of the sheet are virtually undeformable, see the inset in Fig. 2(a), while the center is highly stretchable. When the sheet is stretched by point-like forces, as in Fig. 2(b), the strong geometric incompatibility between the center and the edges produces a global buckling mode spanning the central region and featuring nonzero Gaussian curvature. Note that this buckling instability takes place in tension, unlike in the classical Euler buckling. Increasing the sheet's thickness t, we increase its effective bending modulus and the onset of buckling occurs at larger stretches, as shown in Fig. 2(c). An increased thickness also yields larger deflections and makes the buckled pattern wider, as shown in Fig. 2(d), where we report the lateral extent of the dome *versus* λ_x. These results, further discussed in the ESI,† illustrate that t and λ_x offer some control over the buckled shape and curvature. It is worth pointing out that to obtain buckled patterns as in Fig. 2 it is sufficient to have a variation of stretchability along a single axis (with or without auxeticity), and to apply localized boundary loads along the direction of maximum stretch.

More complex buckling patterns can be obtained by letting both w_x and w_y vary along the sheet, either smoothly or abruptly. In these cases, a sufficient condition to obtain buckled surfaces is the presence of auxetic islands surrounded by unstretchable and non-auxetic regions. As an example, we study the sheet in Fig. 3(a1); when stretched as indicated by the arrows, the two auxetic islands tend to swell biaxially, resulting in strong geometric incompatibilities. This swelling is prevented by the surrounding stiff regions, compressive in-plane stresses arise, and two domes localized on the auxetic islands appear; this is shown numerically and experimentally in Fig. 3(a2). Note that, for this particular cut pattern, a similar buckled shape can be obtained by replacing point loads with distributed boundary loads (see ESI†). As another example, we study the response of a sheet with a more complex cut pattern obtained by varying both w_x and w_y sinusoidally along both the horizontal and vertical directions. The experimental results in (b2) and (b3),

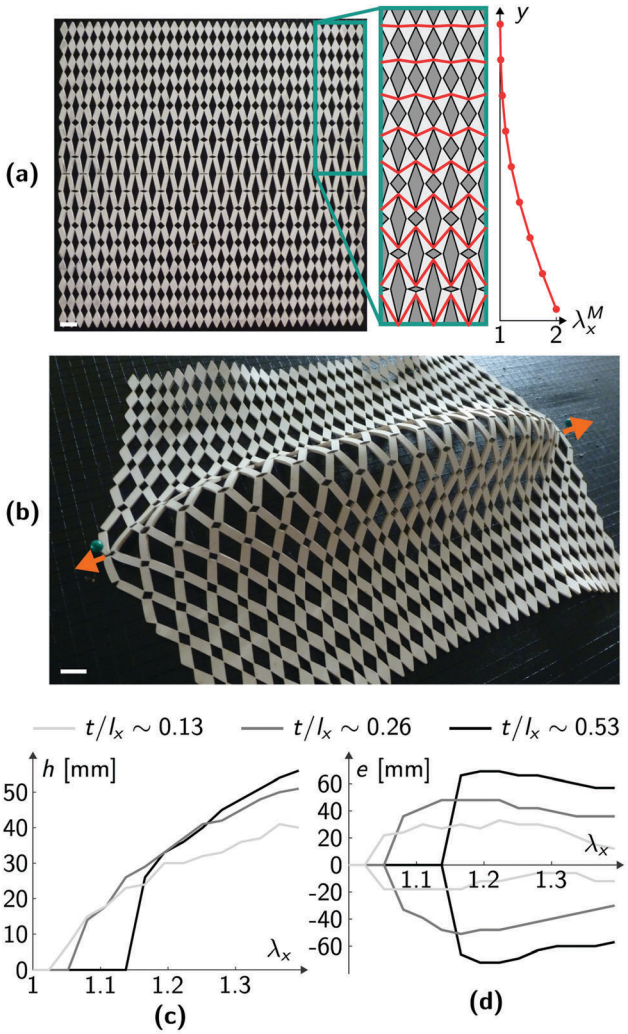

Fig. 2 Out-of-plane morphing of a graded sheet. (a) Cut pattern with gradient in the y-direction. The inset to the right highlights the tile diagonals (in red), and the corresponding maximum kinematic stretch $\lambda_x^M(y)$: the sheet is highly stretchable at the center, but inextensible away from it. (b) A dome shape obtained when the sheet is pulled from two boundary points, as indicated by the arrows. (c) Maximum height and (d) lateral extent of the dome for graded specimens with different thicknesses, for various stretches. Details on how these quantities were measured are given in the ESI.†

corresponding to actuation at the structures' corners or boundary mid-points, respectively, show markedly different wrinkle patterns, thereby highlighting the role of the applied force in selecting the pattern. Finally, in Fig. 3(c1 and c2), we show the response of a sheet featuring a C-shaped auxetic region inserted into an unstretchable sheet. In this case, pulling the specimen as indicated by the orange arrows leads to wrinkles localized along the C-like domain. The wavelength of the wrinkles is comparable to the width of the C-shaped domain. These examples show that the buckling patterns can be tailored by engineering the sheet's local properties through the maps of w_x and w_y, and by choosing the points of application of the load.

Similar principles can be extended to solids of revolution. For example, we pattern a sheet by varying w_x and w_y in vertical

This journal is © The Royal Society of Chemistry 2018

Published on 04 December 2018. Downloaded by California Institute of Technology on 1/31/2019 7:33:55 PM.

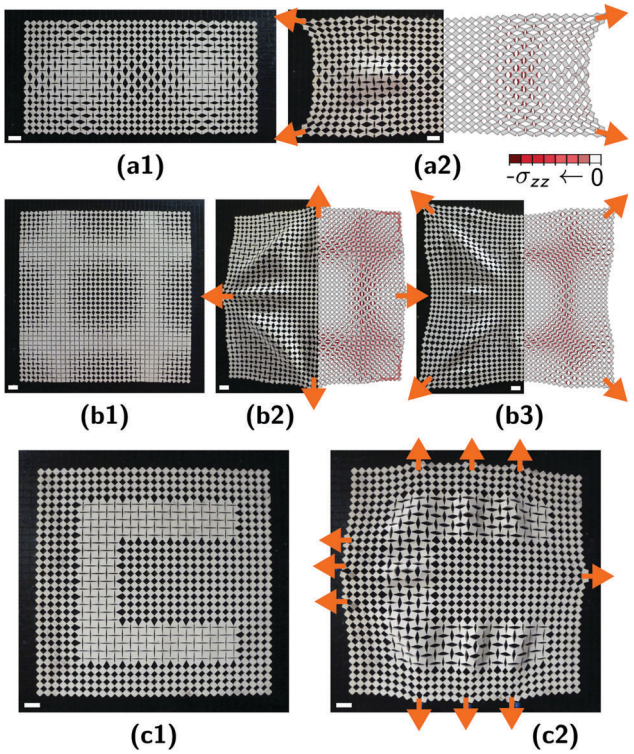

Fig. 3 More complex cut patterns. (a1) Specimen featuring two soft and auxetic regions in its interior, which give rise to two localized bumps upon pulling at the four corners (a2). (b1–b3) Response of another specimen, highlighting the influence of the boundary loading on the surface morphology. The right-halves of (a2), (b2) and (b3) are the stress maps of $\sigma_{zz} = \nu(\sigma_{xx} + \sigma_{yy})$ (under the plane strain assumption); negative values are taken as an indicator for buckling. (c1 and c2) Shaping wrinkles: a C-shaped soft and auxetic region is embedded in a sheet by a suitable choice of the maps of w_x and w_y in the reference configuration (c1). The wrinkles localize upon the application of boundary loads (c2). The arrows indicate the boundary loads. Scale bar: 12 mm.

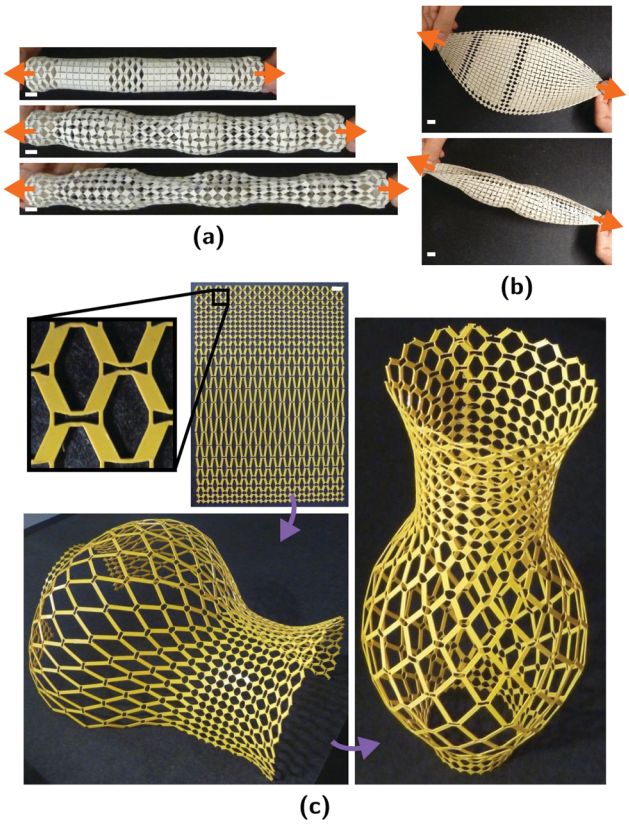

Fig. 4 (a) An architected tube can expand or contract radially based on an initial stripe pattern. Beyond a critical tensile load, an azimuthal buckling pattern appears in the expanded regions. (b) Petal-shaped specimen generated from a non-rectangular grid. This sheet morphs into a pea pod-shaped object when pulled from its ends. (c) Sculpting axisymmetric shapes from a sheet made of an elastic-plastic material; the shapes are obtained by using graded cut patterns and by stretching out the sheets locally by hand. Scale bars: 12 mm.

stripes, alternating regions of auxetic and not-auxetic behavior. We then roll the sheet, forming a tube, and pull on its ends. The applied tractions force the tube to expand at prescribed, auxetic sections and to contract at others,[53] see Fig. 4(a). Stretching the tube further produces a non-axisymmetric buckling bifurcation, with an azimuthal wavelength roughly comparable to the stripes' width. Cut patterns can also be attached to non-Cartesian grids, as illustrated in Fig. 4(b), where the petal-like sheet closes up into a pea pod shape when pulled at its ends.

Finally, permanent three-dimensional shapes can be obtained by using an elastic-plastic material.[36] This requires modifying the hinge design to avoid breakage: the new design, shown in the insets in Fig. 4(c), was inspired by ref. 54 (see ESI†). We leverage the elastic-plastic behavior to sculpt axisymmetric shapes out of a planar PETG sheet, as in Fig. 4(c). As earlier with the tube, this cut pattern is graded along the axis, which allows us to prescribe the radial expansion as a function of the axial coordinate. To obtain an even larger stretchability contrast, we use a non-regular rectangular grid, by setting $l_y(y)$ to take on larger values in the regions of large stretch. The irreversible deformations are obtained by stretching the sheet locally by hand, and a similar effect could be achieved using localized smart-material actuators or pressurized membranes. These structures are reminiscent of gridshells[55] and are easier to fabricate, especially at small scales.

In this work, we have demonstrated that geometric incompatibility can be leveraged to create three-dimensional objects from sheets with non-periodic cut-outs. By choosing the properties of the cuts locally, one can prescribe a map of maximum stretch, which is resolved when the sheet deforms out of plane in response to boundary loads or local stretching. While the shapes we have obtained are relatively simple, similar principles could be extended to different families of mechanisms, and could be coupled to optimization and inverse-design strategies to obtain more complex shapes. Towards this goal, it will be necessary to develop efficient numerical models of these systems and of their buckling behavior—a goal most likely achievable *via* homogenization. In conclusion, our work expands the shape-morphing gamut of perforated mono-layer sheets, and it indicates an approach that could be used to produce morphing and deployable structures at vastly-different scales.

Published on 04 December 2018. Downloaded by California Institute of Technology on 1/31/2019 7:33:55 PM.

Conflicts of interest

There are no conflicts to declare.

Acknowledgements

This research was carried out at the California Institute of Technology and the Jet Propulsion Laboratory under a contract with the National Aeronautics and Space Administration, and funded through the President's and Director's Fund Program. This work is partially supported through the Foster and Coco Stanback Space Innovation Fund. P. C. wishes to thank D. Pasini of McGill University, A. Constantinescu of École Polytechnique, and members of C. D.'s research group for their input and suggestions. We also thank B. Dominguez of Caltech for his assistance during laser cutting.

References

1 Y. Tang and J. Yin, *Extreme Mech. Lett.*, 2017, **12**, 77–85.
2 E. T. Filipov, T. Tachi and G. H. Paulino, *Proc. Natl. Acad. Sci. U. S. A.*, 2015, **112**, 12321–12326.
3 J. T. B. Overvelde, J. C. Weaver, C. Hoberman and K. Bertoldi, *Nature*, 2017, **541**, 347–352.
4 J. N. Grima, V. Zammit, R. Gatt, A. Alderson and K. E. Evans, *Phys. Status Solidi B*, 2007, **244**, 866–882.
5 T. Mullin, S. Deschanel, K. Bertoldi and M. C. Boyce, *Phys. Rev. Lett.*, 2007, **99**, 084301.
6 M. Schenk and S. D. Guest, *Proc. Natl. Acad. Sci. U. S. A.*, 2013, **110**, 3276–3281.
7 J. L. Silverberg, A. A. Evans, L. McLeod, R. C. Hayward, T. Hull, C. D. Santangelo and I. Cohen, *Science*, 2014, **345**, 647–650.
8 L. H. Dudte, E. Vouga, T. Tachi and L. Mahadevan, *Nat. Mater.*, 2016, **15**, 583–588.
9 S. J. P. Callens and A. A. Zadpoor, *Mater. Today*, 2018, **21**, 241–264.
10 E. D. Demaine and T. Tachi, 33rd Int. Symp. on Comput. Geom. (SoCG 2017), 2017, pp. 34:1-34:16.
11 E. Hawkes, B. An, N. M. Benbernou, H. Tanaka, S. Kim, E. D. Demaine, D. Rus and R. J. Wood, *Proc. Natl. Acad. Sci. U. S. A.*, 2010, **107**, 12441–12445.
12 M. Stern, M. B. Pinson and A. Murugan, *Phys. Rev. X*, 2017, **7**, 041070.
13 P. Plucinsky, B. A. Kowalski, T. J. White and K. Bhattacharya, *Soft Matter*, 2018, **14**, 3127–3134.
14 Y. Klein, E. Efrati and E. Sharon, *Science*, 2007, **315**, 1116–1120.
15 J. Kim, J. A. Hanna, M. Byun, C. D. Santangelo and R. C. Hayward, *Science*, 2012, **335**, 1201–1205.
16 Q. Ge, H. J. Qi and M. L. Dunn, *Appl. Phys. Lett.*, 2013, **103**, 131901.
17 T. H. Ware, M. E. McConney, J. J. Wie, V. P. Tondiglia and T. J. White, *Science*, 2015, **347**, 982–984.
18 A. S. Gladman, E. A. Matsumoto, R. G. Nuzzo, L. Mahadevan and J. A. Lewis, *Nat. Mater.*, 2016, **15**, 413–418.
19 H. Aharoni, Y. Xia, X. Zhang, R. D. Kamien and S. Yang, *Proc. Natl. Acad. Sci. U. S. A.*, 2018, **115**, 7206–7211.
20 W. M. van Rees, E. Vouga and L. Mahadevan, *Proc. Natl. Acad. Sci. U. S. A.*, 2017, **114**, 11597–11602.
21 S. M. Felton, M. T. Tolley, B. Shin, C. D. Onal, E. D. Demaine, D. Rus and R. J. Wood, *Soft Matter*, 2013, **9**, 7688–7694.
22 J. H. Na, A. A. Evans, J. Bae, M. C. Chiappelli, C. D. Santangelo, R. J. Lang, T. C. Hull and R. C. Hayward, *Adv. Mater.*, 2014, **27**, 79–85.
23 S. Ahmed, Z. Ounaies and M. Frecker, *Smart Mater. Struct.*, 2014, **23**, 094003.
24 S. Xu, Z. Yan, K. Jang, W. Huang, H. Fu, J. Kim, Z. Wei, M. Flavin, J. McCracken, R. Wang, A. Badea, Y. Liu, D. Xiao, G. Zhou, J. Lee, H. U. Chung, H. Cheng, W. Ren, A. Banks, X. Li, U. Paik, R. G. Nuzzo, Y. Huang, Y. Zhang and J. A. Rogers, *Science*, 2015, **347**, 154–159.
25 Y. Zhang, Z. Yan, K. Nan, D. Xiao, Y. Liu, H. Luan, H. Fu, X. Wang, Q. Yang, J. Wang, W. Ren, H. Si, F. Liu, L. Yang, H. Li, J. Wang, X. Guo, H. Luo, L. Wang, Y. Huang and J. A. Rogers, *Proc. Natl. Acad. Sci. U. S. A.*, 2015, **112**, 11757–11764.
26 M. A. Dias, M. P. McCarron, D. Rayneau-Kirkhope, P. Z. Hanakata, D. K. Campbell, H. S. Park and D. P. Holmes, *Soft Matter*, 2017, **13**, 9087–9092.
27 X. Guo, X. Wang, D. Ou, J. Ye, W. Pang, Y. Huang, J. Rogers and Y. Zhang, *npj Flexible Electron.*, 2018, **2**, 14.
28 D. M. Sussman, Y. Cho, T. Castle, X. Gong, E. Jung, S. Yang and R. D. Kamien, *Proc. Natl. Acad. Sci. U. S. A.*, 2015, **112**, 7449–7453.
29 M. Konaković, K. Crane, B. Deng, S. Bouaziz, D. Piker and M. Pauly, *ACM Trans. Graph.*, 2016, **35**, 89.
30 F. Wang, X. Guo, J. Xu, Y. Zhang and C. Q. Chen, *J. Appl. Mech.*, 2017, **84**, 061007.
31 J. Cui, J. G. M. Adams and Y. Zhu, *Smart Mater. Struct.*, 2017, **26**, 125011.
32 R. M. Neville, F. Scarpa and A. Pirrera, *Sci. Rep.*, 2016, **6**, 31067.
33 H. Fu, K. Nan, W. Bai, W. Huang, K. Bai, L. Lu, C. Zhou, Y. Liu, F. Liu, J. Wang, M. Han, Z. Yan, H. Luan, Y. Zhang, Y. Zhang, J. Zhao, X. Cheng, M. Li, J. W. Lee, Y. Liu, D. Fang, X. Li, Y. Huang, Y. Zhang and J. A. Rogers, *Nat. Mater.*, 2018, **17**, 268–276.
34 M. K. Blees, A. W. Barnard, P. A. Rose, S. P. Roberts, K. L. McGill, P. Y. Huang, A. R. Ruyack, J. W. Kevek, B. Kobrin, D. A. Muller and P. L. McEuen, *Nature*, 2015, **524**, 204–207.
35 T. C. Shyu, P. F. Damasceno, P. M. Dodd, A. Lamoreaux, L. Xu, M. Shlian, M. Shtein, S. C. Glotzer and N. A. Kotov, *Nat. Mater.*, 2015, **14**, 785–789.
36 A. Rafsanjani and K. Bertoldi, *Phys. Rev. Lett.*, 2017, **118**, 084301.
37 Y. Tang, G. Lin, S. Yang, Y. K. Yi, R. D. Kamien and J. Yin, *Adv. Mater.*, 2017, **29**, 1604262.
38 A. Rafsanjani, Y. Zhang, B. Liu, S. M. Rubinstein and K. Bertoldi, *Sci. Rob.*, 2018, **3**, eaar7555.
39 C. Coulais, E. Teomy, K. de Reus, Y. Shokef and M. van Hecke, *Nature*, 2016, **535**, 529–532.
40 R. Guseinov, E. Miguel and B. Bickel, *ACM Trans. Graph.*, 2017, **36**, 64.

 This journal is © The Royal Society of Chemistry 2018

Published on 04 December 2018. Downloaded by California Institute of Technology on 1/31/2019 7:33:55 PM.

41 Y. Cho, J.-H. Shin, A. Costa, T. A. Kim, V. Kunin, J. Li, S. Y. Lee, S. Yang, H. N. Han, I.-S. Choi and D. J. Srolovitz, *Proc. Natl. Acad. Sci. U. S. A.*, 2014, **111**, 17390–17395.
42 J. N. Grima, L. Mizzi, K. M. Azzopardi and R. Gatt, *Adv. Mater.*, 2016, **28**, 385–389.
43 A. Ion, J. Frohnhofen, L. Wall, R. Kovacs, M. Alistar, J. Lindsay, P. Lopes, H.-T. Chen and P. Baudisch, UIST '16, 2016, pp. 529–539.
44 M. J. Mirzaali, S. Janbaz, M. Strano, L. Vergani and A. A. Zadpoor, *Sci. Rep.*, 2018, **8**, 965.
45 E. Efrati, E. Sharon and R. Kupferman, *J. Mech. Phys. Solids*, 2009, **57**, 762–775.
46 A. Boudaoud, *Trends Plant Sci.*, 2010, **15**, 353–360.
47 M. Osterfield, X. Du, T. Schüpbach, E. Wieschaus and S. Y. Shvartsman, *Dev. Cell*, 2013, **24**, 400–410.
48 A. Rafsanjani and D. Pasini, *Extreme Mech. Lett.*, 2016, **9**, 291–296.
49 S. Pellegrino and C. Calladine, *Int. J. Solids Struct.*, 1986, **22**, 409–428.
50 C. Coulais, C. Kettenis and M. van Hecke, *Nat. Phys.*, 2017, **14**, 40–44.
51 R. G. Hutchinson and N. A. Fleck, *J. Mech. Phys. Solids*, 2006, **54**, 756–782.
52 V. Kapko, M. M. J. Treacy, M. F. Thorpe and S. D. Guest, *Proc. R. Soc. London, Ser. A*, 2009, **465**, 3517–3530.
53 J. Liu and Y. Zhang, *Soft Matter*, 2018, **14**, 693–703.
54 X. Shang, L. Liu, A. Rafsanjani and D. Pasini, *J. Mater. Res.*, 2018, **33**, 300–308.
55 C. Baek, A. O. Sageman-Furnas, M. K. Jawed and P. M. Reis, *Proc. Natl. Acad. Sci. U. S. A.*, 2018, **115**, 75–80.